

Study on the pointing model of a slant-axis terahertz antenna

Yu Wang^{1,3}, Zheng Lou^{1,2}, Ying-Xi Zuo^{1,2}, Hao-Ran Kang^{1,4} and Ming-Zhu Zhang^{1,4}

¹ Purple Mountain Observatory, Chinese Academy of Sciences, Nanjing 210034, China; zhenglou@pmo.ac.cn

² Key Laboratory for Radio Astronomy, Chinese Academy of Sciences, Nanjing 210034, China

³ Shanghai Normal University, Shanghai 201400, China

⁴ University of Science and Technology of China, Hefei 230026, China

Received 2019 July 19; accepted 2019 December 16

Abstract This paper describes the establishment and verification of an accurate pointing model for a 1.2 m aperture slant-axis terahertz antenna. A new analytical pointing model for the slant-axis antenna is presented based on an analogy to that of the alt-azimuth antennas. Furthermore, extra error terms are added to the pointing model based on the structure and mechanical analysis of the slant-axis antenna. To verify the pointing model experimentally, a pointing error measurement method based on photogrammetric techniques is proposed. Using this method, pointing behaviors of the antenna are accurately measured without the aid of astronomical observations, and major sources of the pointing errors are measured individually by photogrammetry and their respective coefficients are compared with those in the analytical pointing model. The results show that an extended pointing model consisting 21 error terms can significantly reduce the residual systematic errors compared with the traditional model, more details are given in the following sections.

Key words: telescopes — slant-axis antenna — photogrammetry — pointing models

1 INTRODUCTION

To explore the terahertz (THz) astronomical science by taking advantage of the excellent atmospheric transparency and stability at Dome A in Antarctica, 5 meter Dome A Terahertz Explorer (DATE5) was proposed (Yang et al. 2013). Figure 1 gives the conceptual design of the telescope. DATE5 features an unusual slant-axis mount design. Due to its unique rotation mechanism, DATE5 can be covered with a smooth thermal cladding and offer better adaptability to extreme site conditions such as Antarctica as compared to traditional equatorial or alt-azimuth mounts. Moreover, the azimuth and slant axes use identical mechanics and the same type of bearings, gears and encoders, which simplifies the design of the antenna mount and reduces the costs. Some studies have been performed on the motion characteristics and drive control methods for slant-axis antenna (Liu 2015; Zhou et al. 2017). Due to the non-orthogonality of its axes system, the motion characteristics of the slant mount is more complicated than alt-azimuth mount and needs more devoted studies.

Pointing accuracy is one of the most important specifications for astronomical telescopes. The requirement for

deviation from exact pointing is usually less than 10% of the antenna's half-power beam width (Levy 1996). For DATE5, the blind pointing error should be no more than 2'' rms. In general, the actual pointing of an antenna always deviates from the command of the host computer by some extent. Both systematic and random errors contribute to the overall pointing error. The systematic components are usually compensated by the use of a pointing model. Various analytical pointing models that consider linear and nonlinear errors have been applied for the pointing calibration of most large radio antennas (Gao et al. 2007; Greve et al. 1996; Kong et al. 2014; Meeks et al. 1968). However, due to the non-orthogonality between slant and azimuth axes, the analytical models for alt-azimuth or equatorial antenna are not suitable for slant-axis antenna anymore. Therefore, a new analytical pointing model tailored for slant-axis antennas is proposed in this study.

For radio telescopes, pointing errors are usually measured by five-point observation or cross scan on radio point sources whose precise locations are known (Kang et al. 2018; Yu et al. 2015). But at THz bands there are very few point sources available for pointing measurements and usually they do not provide full sky coverage. Meanwhile,

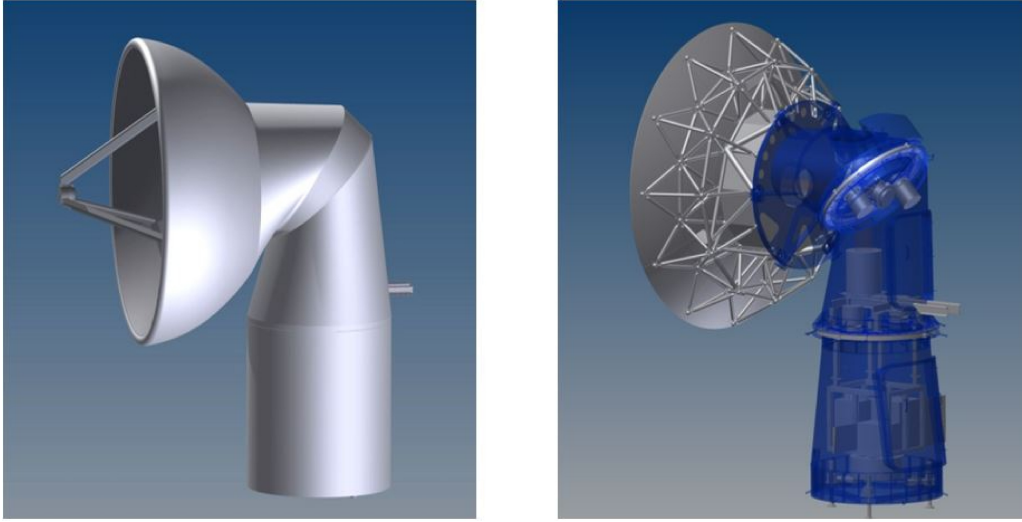


Fig. 1 The conceptual design of the 5m Dome A Terahertz telescope (DATE5) with cladding (*left*) and without cladding (*right*).

pointing errors of a radio telescope may be caused by the misalignment and deformation of the antenna, the Earth's atmospheric fluctuation, and receiver feeds misalignment, etc. Among them, the error sources related to the antenna itself mainly include encoder errors, axis errors, and gravitational deflection error, etc., and the calibration of these errors does not require observation of the astronomical point sources. For example, the ALMA European antenna utilizes inclinometers to measure the deflection of the elevation axis under wind and temperature loads (Rampini & Marchiori 2012) and the Tianma 65m antenna uses micrometer to measure the elevation backlash (Wang et al. 2017). In this research, a pointing measurement method based on photogrammetric techniques is developed to measure the major error sources related to the antenna itself. The advantage of this method is that it involves no observations of astronomical sources, which means the pointing error can be measured for the full sky with equal precision, and it puts no requirements on the initial pointing and surface accuracy of the antenna under test. Furthermore, it can separate the major error sources such as axis misalignment and encoder zero offset from the overall pointing model of the antenna, providing a more accurate and physical basis for the establishment and optimization of the final pointing model.

The pointing error models can be categorized as the analytical model, the spherical harmonic model, and the neural network model (Penalver et al. 2000; Yu et al. 2016; Zhu et al. 2013). The analytical model can describe the physical sources of the pointing errors and has analytical expressions. However, it cannot account for all kinds of error sources, especially those high-order terms. As for spherical harmonic model, although it can include more kinds of errors, the parameters of the model are highly cor-

related (Zhao 2008). The accuracy of neural network model relies heavily on the amount and accuracy of data. In this research, the analytical model is adopted because it is easier to converge, the fitting coefficients are more stable, and the physical meaning is clearer compared with other models.

Section 2 describes the structure of the slant-axis antenna and proposes a seven-term analytical pointing model for such an antenna. Section 3 introduces the measurement method of pointing error based on photogrammetry and verifies the accuracy of the method. In Section 4, the experimental study of a 1.2 m slant-axis terahertz antenna is described, and, based on the results, an extended pointing model is established. Finally, a summary is presented in Section 5.

2 ANALYTICAL POINTING MODELS

The widely used pointing model for an alt-azimuth antenna includes seven error terms (Baars et al. 2007; Cheng 2003; Zhang & Wu 2001), and the pointing errors in azimuth and elevation can be expressed as

$$\begin{cases} \Delta_{AZ} = C_1 \tan \theta \sin \phi + C_2 \tan \theta \cos \phi + C_3 \tan \theta \\ \quad + C_4 \sec \theta + C_5, \\ \Delta_{EL} = C_1 \cos \phi + C_2 \sin \phi + C_6 + C_7 \cos \theta. \end{cases} \quad (1)$$

where Δ_{AZ} and Δ_{EL} are the azimuth and elevation pointing errors separately, θ and ϕ are the elevation (EL) and azimuth (AZ) angles, C_1 is the AZ axis north-south misalignment error, C_2 is the AZ axis east-west misalignment error, C_3 is the non-perpendicularity error between EL and AZ axes, C_4 is the non-perpendicularity error between EL axis and main beam (BM), C_5 is the AZ encoder zero offset, C_6 is the EL encoder zero offset, and C_7 is the gravitational deflection error.

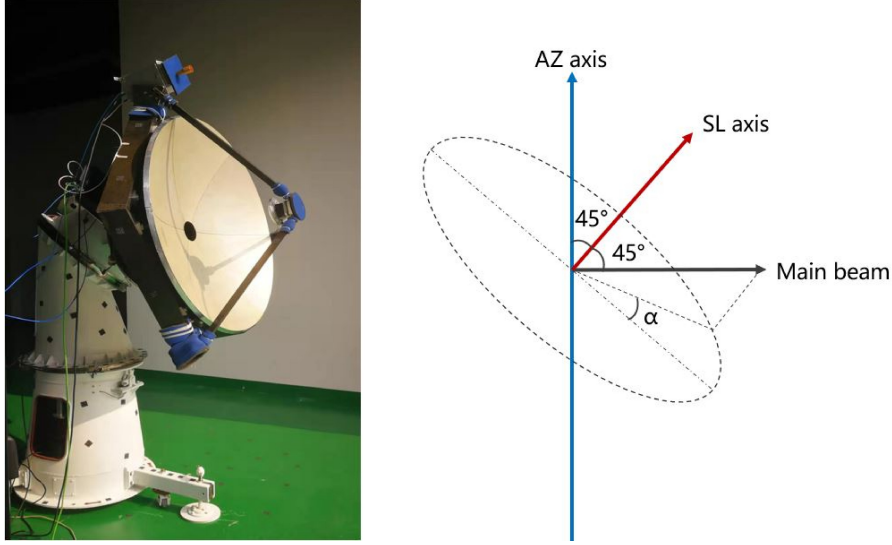


Fig. 2 The slant-azimuth mount system. Photo of the 1.2 m slant-axis antenna (left), geometry of the axes (right).

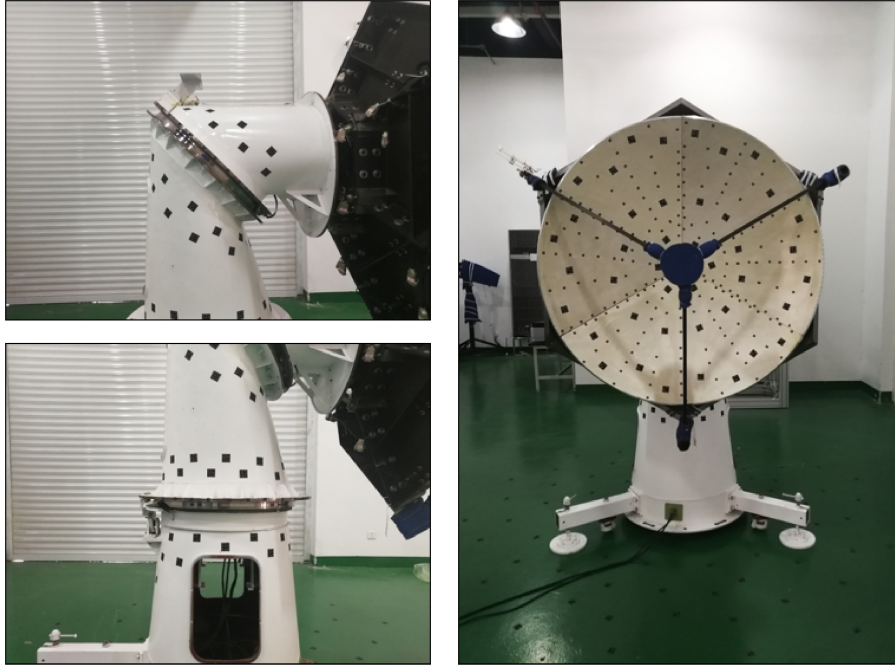


Fig. 3 The RRT on the 1.2 m slant-axis antenna.

Figure 2 shows the photo and the axis geometry of the 1.2 m slant-axis antenna. It can be seen that the slant is 45 degrees with respect to both the azimuth axis and antenna main beam. This means that the rotation of the slant axis will cause both azimuth and elevation angle changes. The transformation from slant-azimuth coordinates (α, β) to the elevation-azimuth coordinates (θ, ϕ) can be expressed as (Lou et al. 2015)

$$\begin{cases} \theta = \sin^{-1}(\sin^2 \frac{\alpha}{2}), \\ \phi = \beta + \tan^{-1}(\sqrt{2} \tan \frac{\alpha}{2}), \end{cases} \quad (2)$$

where α and β are slant and azimuth coordinates. By an analogy to the seven-term analytical pointing model for an alt-azimuth antenna (Eq. (1)), an analytical model for a slant-axis antenna is derived as

$$\begin{cases} \Delta_{AZ} = -C_1 \tan \theta \sin \phi + C_2 \tan \theta \cos \phi \\ \quad + C_3 \frac{\sqrt{2} \sin \alpha (1 - \cos \alpha)}{\sin^2 \alpha + 2 \cos \alpha + 2} - C_4 \frac{2\sqrt{2} \sin \alpha}{\sin^2 \alpha + 2 \cos \alpha + 2} \\ \quad - C_5 - C_6 \frac{1}{\sqrt{2}(1 + \sin \theta)}, \\ \Delta_{EL} = -C_1 \cos \phi - C_2 \sin \phi + (C_3 + C_4) \frac{\sin \theta - 1}{\cos \theta} \\ \quad + C_6 \frac{\sin \alpha}{2 \cos \theta} - C_7 \cos \theta, \end{cases} \quad (3)$$

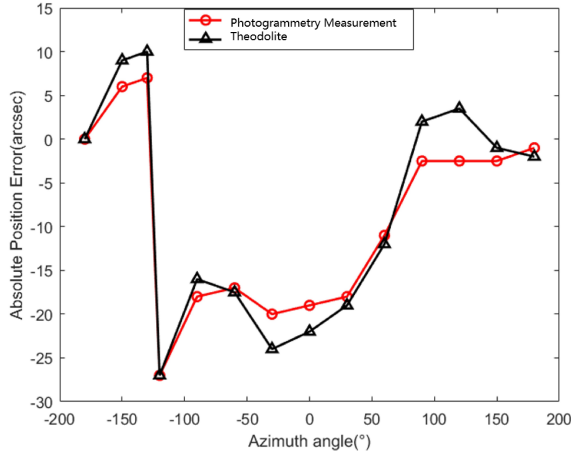


Fig. 4 Comparison of photogrammetry and theodolite.

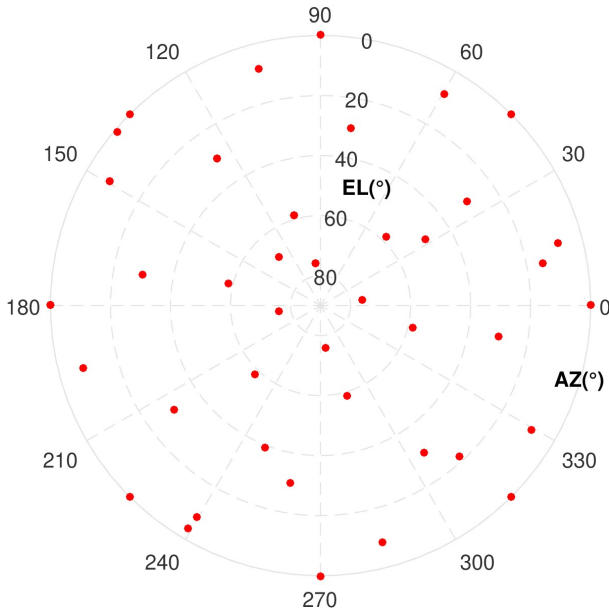


Fig. 5 The sky coverage of the pointing measurements.

where C_1 is the AZ axis north-south misalignment error, C_2 is the AZ axis east-west misalignment error, C_3 is the error caused by the angle between slant (SL) and AZ axes not equal to 45° , C_4 is the error caused by the angle between SL and BM not equal to 45° , C_5 is the AZ encoder zero offset, C_6 is the SL encoder zero offset, and C_7 is the gravitational deflection. Finally, the overall pointing accuracy Δ_{tot} of the antenna can be expressed as

$$\Delta_{\text{tot}} = \sqrt{(\Delta_{\text{AZ}}^2 \cos^2 \text{EL} + \Delta_{\text{EL}}^2)}. \quad (4)$$

3 POINTING MEASUREMENT TECHNIQUE

3.1 Photogrammetric Measurement

In our experimental studies, a pointing error measurement method based on photogrammetry is developed and ap-

plied to obtain the pointing error of the antenna under investigation. Digital photogrammetry has been used to automatically acquire geometric information from the optical images of the object to be measured and extract the digitized model (Fraser 1992). Typical photogrammetric process involves following steps (Fan et al. 2010). First, apply the retro-reflective targets (RRT) to the reflective surface and the key parts of the antenna. Then, take the digital photos of the RRT on the antenna at different angles and process the optical images to get the 3D coordinates of the measuring point. In radio astronomy, photogrammetry is widely used to measure the surface figure of the antenna reflectors. In this research, the technique is extended to measure the pointing behavior of the antenna.

Before the measurement, RRT are applied to the reflector surface and key structure components of the antenna under investigation. Figure 3 shows the RRT on the 1.2 m slant-axis antenna. The RRT on the reflector system are used to extract the overall pointing error. The RRT near the slant and azimuth bearings are used to measure the individual axis and encoder error respectively. The RRT on the antenna foundation and ground are used as references with fixed positions.

After obtaining the 3D coordinates of the RRT on the reflector system and key parts of the antenna at different pointing angles, the overall pointing error as well as the information of individual antenna axes can be extracted using the following algorithm:

(1) The coordinates on the reflector system at $[\text{AZ}, \text{SL}] = (0, 0)$ are chosen as the reference data set. The RRT coordinates at a specific pointing are then compared with the reference data set and the rotation angles between the two data sets are found by a least square fitting. Finally, the pointing error is calculated as the difference between the command and the actual rotation angles.

(2) The coordinates on the azimuth bearing at different azimuth angles are used to determine the actual azimuth axis and the azimuth encoder error. A similar process is then applied to the slant axis.

(3) Moreover, the axis misalignment errors are found by calculating the actual directions of the axes and compared them with the designed values.

3.2 Measurement Accuracy

Before applying this new measurement method, extensive verification experiments were carried out to demonstrate its accuracy and reliability. First, repeated measurements are performed to verify the repeatability of the method. At command $[\text{AZ}, \text{SL}] = (0, 0)$, the antenna's actual pointing was measured for 12 times. Table 1 gives the results of each measurements with respect to the mean value.

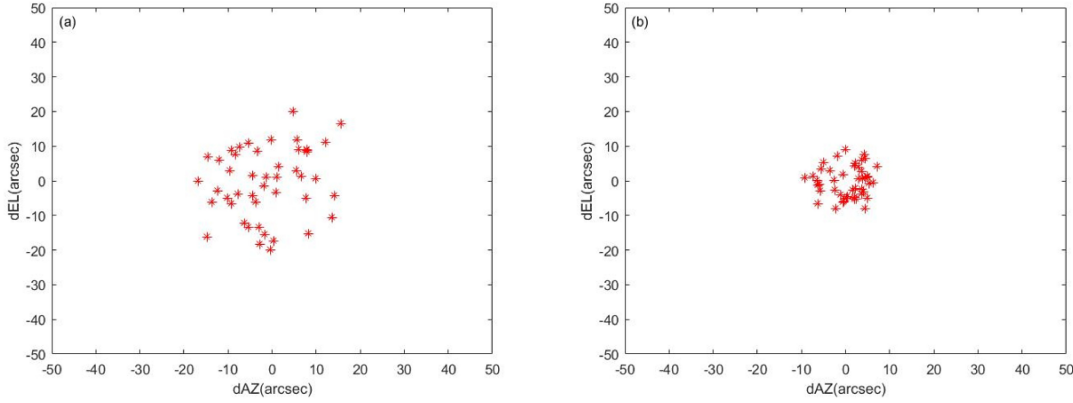


Fig. 6 The distribution of pointing calibration residuals. (a) The traditional model including seven error terms (Eq. (3)), (b) the extended model including 21 error terms (Eq. (5)).

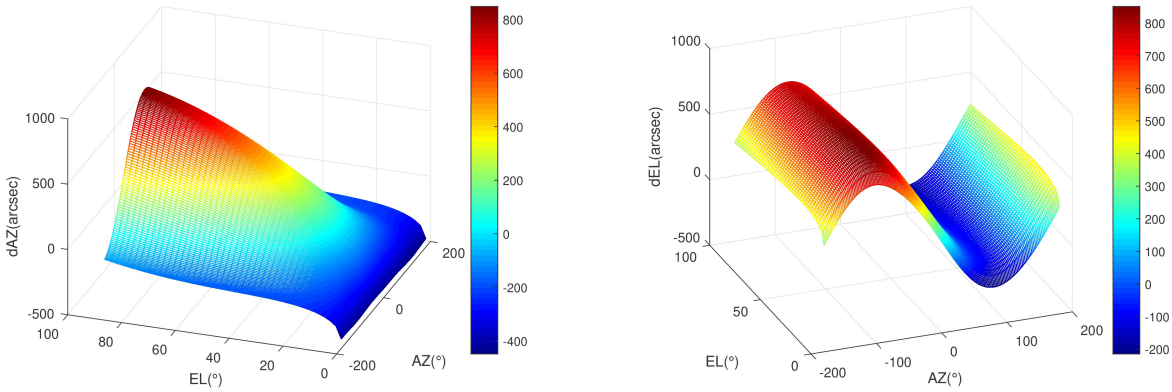


Fig. 7 The calibration surface of the extended pointing model: azimuth (*left*) and elevation (*right*).

Table 1 Repeated Measurements

Number	$\Delta_{AZ}(\prime\prime)$	$\Delta_{EL}(\prime\prime)$
1	-0.48	-1.46
2	-0.14	2.33
3	1.36	-0.37
4	-1.67	1.33
5	-0.48	1.46
6	-0.14	2.33
7	-1.24	-0.12
8	-1.46	1.08
9	-0.12	-0.91
10	-1.10	0.94
11	-0.29	0.84
12	2.76	0.21
RMS	1.22	1.31

As shown in Table 1, the RMS repeatability error is 1.22'' for azimuth and 1.31'' for elevation. Considering the repositioning accuracy of the antenna mount is 3'' RMS, the repeatability of the measurement alone is reasonably good. In addition, the encoder error measured by the photogrammetric method is compared with that by the theodolite measurement, and the results are shown in Figure 4. It

is worth mentioning that the sharp notch near -130° is due to the switching of the two azimuth encoder readers.

It can be seen from Figure 4 that the two measurement methods have good consistency. In the following section, the photogrammetric method is therefore used to study the pointing behavior of the 1.2 m slant-axis terahertz antenna.

4 EXPERIMENTAL RESULTS

The pointing model verification experiment is based on the 1.2 m slant-axis terahertz antenna developed by Purple Mountain Observatory. Figure 5 shows the sky coverage of the pointing measurements. A total of 46 samples are measured. The $[AZ, SL] = (0, 0)$ position is used as the reference position where both AZ and SL encoder readings are equal to zero, and has been measured 12 times to guarantee its accuracy. Multiple measurements were taken and averaged at each sample point to ensure the reliability and accuracy of the data.

After obtaining the pointing errors at different command angles and fitting the pointing error with the seven-term analytical model, the rms residual pointing error is

Table 2 Error Sources for the Extended Pointing Model

Error Term	Error Source
$C_1 \sim C_7$	Same as Equation (3)
C_8, C_9, C_{16}, C_{17}	Structural deformation due to two cabin doors
$C_{10}, C_{11}, C_{18}, C_{19}$	Structural deformation due to tripod legs
C_{12}	Radius error of the AZ encoder
C_{13}, C_{14}	Decenter errors of the AZ encoder
C_{15}	Radius error of the SL encoder
C_{20}, C_{21}	Decenter errors of the SL encoder

Table 3 Comparison of the Pointing Error Coefficients

Item	Coefficients by separate measurement(")	Coefficients by model fitting(")
AZ tilt(north-south) error	62.02	71.40
AZ tilt(east-west) error	459.06	463.12
AZ-SL angle error	20.42	26.41
SL-BM angle error	-368.28	-363.40
AZ encoder zero-error	85.84	92.08
SL encoder zero-error	484.90	484.10

Table 4 Comparison of the Pointing Residuals (RMS) of the 1.2 m Slant-Axis Antenna

Item	δ_1 (")	δ_2 (")	δ_3 (")	δ_4 (")
Azimuth	312.00	9.56	3.71	5.26
Elevation	453.77	8.46	4.29	8.69
Total	550.68	13.06	5.67	10.17

reduced from 550.68'' to 13.06''. It proves the validity of the model, but the accuracy is not sufficient. By examining the residual pointing errors of the seven-term model, we can easily identify some high-order terms which represents some uncorrected systematic errors. For example, we find two-fold and tri-fold patterns in the elevation errors with respect to the azimuth angle. We believe that they are related to the structure deformations caused by the two cabin doors and three tripod legs, respectively. Moreover, for the strip encoder we use, we already know the inaccuracy in the encoder radius may cause azimuth and slant-axis angle errors that grow linearly with the encoder readings. By adding these higher-order terms to Equation (3), we arrive at an extended pointing model consisting of 21 error terms, which can be expressed as Equation (5). The error sources for these terms are summarized in Table 2.

$$\left\{ \begin{array}{l} \Delta_{AZ} = -C_1 \tan \theta \sin \phi + C_2 \tan \theta \cos \phi \\ \quad + C_3 \frac{\sqrt{2} \sin \alpha (1 - \cos \alpha)}{\sin^2 \alpha + 2 \cos \alpha + 2} - C_4 \frac{2\sqrt{2} \sin \alpha}{\sin^2 \alpha + 2 \cos \alpha + 2} \\ \quad - C_5 - C_6 \frac{1}{\sqrt{2}(1 + \sin \theta)} + C_{12} \phi \\ \quad + C_{13} \cos \phi + C_{14} \sin \phi - C_{15} \frac{\alpha}{\sqrt{2}(1 + \sin \theta)} \\ \quad + C_{16} \cos(2\phi) + C_{17} \sin(2\phi) \\ \quad + C_{18} \sin(3\beta) + C_{19} \cos(3\beta), \\ \Delta_{EL} = -C_1 \cos \phi - C_2 \sin \phi + (C_3 + C_4) \frac{\sin \theta - 1}{\cos \theta} \\ \quad + C_6 \frac{\sin \alpha}{2 \cos \theta} - C_7 \cos \theta + C_8 \cos(2\beta) \cos \theta \\ \quad + C_9 \sin(2\beta) \cos \theta + C_{10} \sin(3\beta) \cos \theta \\ \quad + C_{11} \cos(3\beta) \cos \theta + C_{15} \frac{\alpha \sin \alpha}{2 \cos \theta} \\ \quad + C_{20} \sin \phi \cos \theta + C_{21} \cos \phi \cos \theta. \end{array} \right. \quad (5)$$

As compared to the seven-term analytical model, the rms pointing error of the extended model decreases from 13.06'' to 5.67'', which improves by 56.6%. Figure 6 shows the distribution of residual errors after the pointing calibration based on the two analytical pointing models, Equations (3) and (5), respectively. As shown, the latter's residual error obviously decreases, with maximum error less than 10''.

Moreover, some major error sources can be separated and characterized individually by photogrammetry. The measured AZ axis misalignment error is 62.02'' to the south and 459.06'' to the west. The angle between AZ and SL axes is 45.0057° which is deviated from 45° by 20.42''. The angle between SL axis and BM axis is 44.9216° which is deviated from 45° by -282.15''. Table 3 gives the comparison of the coefficients obtained by separate measurement and model fitting from Equation (5). It can be seen that there is a high consistency between the two sets of coefficients which proves the reliability of the pointing model and the measurement method. Note that the SL-BM angle error in Table 3 is not equal to -282.15''. This happens because it also includes the gravitational deflection of 86.13''. Figure 7 shows the calibration surface of the extended model including encoder radius and decenter errors and some high-order errors due to the antenna mechanical imperfections.

For comparison purposes, a spherical harmonic model is also used to fit the pointing and compared with the analytical model. The spherical harmonic model used in this

study is expressed as (Zhao 2008; Zheng et al. 2003):

$$\left\{ \begin{array}{l} \Delta_{AZ} \cos(\text{EL}) = A_1 + A_2 \sin \theta + A_3 \cos \phi \sin \theta \\ \quad + A_4 \sin \phi \sin \theta + A_5 \sin^2 \theta + A_6 \cos \phi \cos \theta \sin \theta \\ \quad + A_7 \sin \phi \cos \theta \sin \theta + A_8 \sin^3 \theta \\ \quad + A_9 \cos \phi \cos \theta \sin^2 \theta + A_{10} \sin \phi \cos \theta \sin^2 \theta \\ \quad + A_{11} \sin^4 \theta + A_{12} \cos \phi \cos \theta \sin^3 \theta \\ \quad + A_{13} \sin \phi \cos \theta \sin^3 \theta + A_{14} \sin^5 \theta \\ \quad + A_{15} \cos \phi \cos \theta \sin^4 \theta + A_{16} \sin \phi \cos \theta \sin^4 \theta, \\ \Delta_{EL} = B_1 + B_2 \sin \theta + B_3 \cos \phi \cos \theta + B_4 \sin \phi \cos \theta \\ \quad + B_5 \sin^2 \theta + B_6 \cos \phi \cos \theta \sin \theta \\ \quad + B_7 \sin \phi \cos \theta \sin \theta + B_8 \sin^3 \theta \\ \quad + B_9 \cos \phi \cos \theta \sin^2 \theta + B_{10} \sin \phi \cos \theta \sin^2 \theta \\ \quad + B_{11} \sin^4 \theta + B_{12} \cos \phi \cos \theta \sin^3 \theta \\ \quad + B_{13} \sin \phi \cos \theta \sin^3 \theta \\ \quad + B_{14} \sin^5 \theta + B_{15} \cos \phi \cos \theta \sin^4 \theta \\ \quad + B_{16} \sin \phi \cos \theta \sin^4 \theta + B_{17} \sin^6 \theta \\ \quad + B_{18} \cos \phi \cos \theta \sin^5 \theta + B_{19} \sin \phi \cos \theta \sin^5 \theta. \end{array} \right. \quad (6)$$

Results of the pointing calibration for the 1.2 m slant-axis antenna are shown in Table 4, where δ_1 is the error before calibration, δ_2 is the residual pointing error after calibration using the basic seven-term model (Eq. (3)) which only considers some basic error sources, δ_3 is the residual pointing error after calibration using the extended pointing model (Eq. (5)) which includes 21 error items, and δ_4 is the residual pointing error using the spherical harmonic model (Eq. (6)). It can be seen from Table 4 that the extended pointing model that includes encoder decenter and radius errors and some high-order errors is significantly better than the basic analytical model and the spherical harmonic model.

5 SUMMARY

The pointing model for a slant-axis terahertz antenna is studied both theoretically and experimentally. A basic seven-term pointing model is first derived by an analogy to that of an alt-azimuth antenna. Moreover, an extended pointing model considering encoder decenter and radius errors and some high-order structural deformation errors is proposed based on the measurement results of a 1.2 m slant-axis terahertz antenna. The results show that the extended model can effectively correct the residual pointing errors due to the antenna mechanical imperfections. The overall pointing error is reduced by 56.6% compared to the basic seven-term model. The extended model also shows superior accuracy as compared to the spherical harmonic model.

Moreover, a pointing error measurement method based on photogrammetry is proposed and verified. This method can be used to measure and characterize the pointing errors related to the antenna itself without resorting to as-

tronomical observations. Therefore, it is suitable for THz telescopes where THz point sources available for pointing measurements is scarce, and also suitable for antennas still in the alignment and testing phase. Furthermore, this method allows major error sources such as axis misalignment and encoder errors to be separated and characterized individually. Repeatability experiments show that angular accuracy of one arcsecond can be achieved, independent of the antenna's aperture size.

This paper focuses on the pointing performance of the slant-axis antenna itself. It should be noted that the overall pointing model of the telescope should include more error terms to correct atmospheric refraction and receiver feed offset, etc. However, these terms are the same as for the traditional alt-azimuth telescopes. Therefore, they are not discussed in this paper. Verification of the overall telescope pointing model by the observation of astronomical point sources is under plan and will be conducted in the near future.

Acknowledgements This work was supported in part by the National Key Basic Research and Development Program (Grant No. 2018YFA0404702) and in part by National Natural Science Foundation of China (Grant Nos. 11673074 and 11773084).

References

- Baars, J. W. M., Lucas, R., Mangum, J. G., & Lopez-Perez, J. A. 2007, *IEEE Antennas and Propagation Magazine*, 49, 24
- Cheng, J. 2003, *The Principles of Astronomical Telescope Design* (1st ed., Beijing: China Science and Technology Press)
- Fan, Q. H., Fang, S. H., Zuo, Y. X., et al. 2010, *Acta Astronomica Sinica*, 51, 210
- Fraser, C. S. 1992, *Photogrammetric Engineering and Remote Sensing*, 58, 305
- Gao, G.-N., Wang, M., Shi, S.-B., et al. 2007, *Publications of the National Astronomical Observatories of China*, 4, 188
- Greve, A., Panis, J. F., & Thum, C. 1996, *A&AS*, 115, 379
- Kang, H. R., Zuo, Y. X., Lou, Z., & He, Q. R. 2018, *Acta Astronomica Sinica*, 59, 17
- Kong, D.-Q., Wang, S.-G., Wang, J.-Q., Wang, M., & Zhang, H.-B. 2014, *RAA (Research in Astronomy and Astrophysics)*, 14, 733
- Levy, R. 1996, *Structural Engineering of Microwave Antennas for Electrical, Mechanical, and Civil Engineers* (Piscataway, NJ: IEEE Press, —c1996)
- Liu, W. 2015, *Dirving Control for the Slant-axis Mount of Astronomical Telescopes*, PhD thesis, Nanjing University of Information Science and Technology
- Lou, Z., Cheng, J. Q., Zuo, Y. X., & Yang, J. 2015, *Acta Astronomica Sinica*, 56, 189

- Meeks, M. L., Ball, J. A., & Hull, A. B. 1968, *IEEE Transactions on Antennas and Propagation*, 16, 746
- Penalver, J., Lisenfeld, U., & Mauersberger, R. 2000, *Pointing with the IRAM 30-m Telescope*, in *Society of Photo-Optical Instrumentation Engineers (SPIE) Conference Series*, 4015, ed. H. R. Butcher, 632
- Rampini, F., & Marchiori, G. 2012, in *SPIE Conference Series*, 8450, *Results of the New Metrology System of the European ALMA Antenna*, 84500T
- Wang, J., Yu, L., Zhao, R., et al. 2017, *Scientia Sinica Physica, Mechanica & Astronomica*, 47, 129504
- Yang, J., Zuo, Y.-X., Lou, Z., et al. 2013, *RAA (Research in Astronomy and Astrophysics)*, 13, 1493
- Yu, L. F., Wang, J. Q., Zhao, R. B., et al. 2015, *Acta Astronomica Sinica*, 56, 165
- Yu, Y. Z., Han, L., Zhou, S., et al. 2016, *Astronomical Research and Technology (in Chinese)*, 13, 408
- Zhang, X. X., & Wu, L. D. 2001, *Acta Astronomica Sinica*, 42, 198
- Zhao, Y. 2008, *Research on Modeling Analysis and Design of Pointing Errors for Large Radio Telescope*, PhD thesis, Xian: Xidian University
- Zheng, X. M., Wang, W., Zhang, Y. C., & Feng, H. S. 2003, *Acta Astronomica Sinica*, 44, 330
- Zhou, W. P., Wang, Y., & Gong, L. F. 2017, *Computer Simulation (in Chinese)*, 34, 259
- Zhu, C. G., Guo, T. Y., Zou, T., et al. 2013, *Journal of Geodesy and Geodynamics*, 33, 150